Journal of Materials Chemistry B

Accepted Manuscript

ROYAL SOCIETY OF CHEMISTRY

www.rsc.org/materialsB

Journal of Materials Chemistry B

Journal of Materials Chemistry B

Dynamic Article Links ►

Cite this: DOI: 10.1039/coxx00000x

PAPER

www.rsc.org/xxxxxx

Enhanced Colloidal Stability and Antibacterial Performance of Silver Nanoparticles/Cellulose Nanocrystal Hybrids

Zengqian Shi,[a] Juntao Tang,[a] Li Chen, [a] Chuanren Yan,[a] Shazia Tanvir,[a] William A. Anderson,[a] Richard M. Berry[b] and Kam C Tam*[a]

Received (in XXX, XXX) Xth XXXXXXXXX 20XX, Accepted Xth XXXXXXXXX 20XX
DOI: 10.1039/b000000x

The aggregation of nanoparticles has been shown to significantly reduce the activity of nanomaterials, resulting in inferior performance. As an alternative to the use of traditional capping agents, stabilization of unstable nanoparticles with water-dispersible and biocompatible nanopaticle is a promising strategy. A bioinspired coating strategy was developed and the hybrid nanoparticles displayed excellent colloidal stability that significantly improved antibacterial activity when silver nanoparticles (AgNPs) was used as model particles. Cellulose nanocrystals (CNC) were first modified with dopamine, followed by in-situ generation and anchoring of AgNPs on the surface of CNC through the reduction of silver ions by polydopamine coated CNC. The results indicated that the dispersion stability of AgNPs was significantly enhanced by CNC, which in turn resulted in more than fourfold increase in antibacterial activity based on antibacterial studies using *Escherichia coli* and *Bacillus subtilis*.

Introduction

Various nanoparticles have been explored for many different applications due to their versatile benefits and virtues. For instance, silver nanoparticles (AgNPs) were used as antibacterial agents,[1–4] conductive adhesives, high-intensity LEDs,[5–7] metal-enhanced fluorescence (MEF),[8] surface-enhanced Raman scattering (SERS)[9] and catalysts for dye degradation.[10–12] They are ideal model nanoparticles to investigate stability and catalyst performance. Although the mechanisms of killing microbes by Ag ions and AgNPs are not fully understood, the remarkable antibacterial property of Ag has been known for centuries.[13] Some studies have demonstrated that it might result from a combined effect of cell wall collapse, disruption of respiratory functions, and further damage towards proteins and DNA.[13, 14–16] This combined mechanism prohibits microbes from mutating or developing antibiotic resistance to silver ions and AgNPs, which is a serious and growing concern for other chemical antimicrobial agents.[17] With high activity against a wide range of bacteria, AgNPs have been widely used in water purification,[18] food preservation,[19] wound dressings,[20] and cosmetics,[21] having low toxicity to human cells, high thermal stability and low volatility.[22]

AgNPs are commonly fabricated through the reduction of silver nitrate and are stabilized by capping agents to minimize aggregation arising from the high surface areas of nanoparticles. Common capping agents used include citrates,[23] oleic acids,[24] polysaccharides,[25] sophorolipids,[26] gum Arabic,[27] surfactants, such as sodium dodecyl sulphate (SDS), cetyltrimethylammonium bromide (CTAB), and polyoxyethylenesorbitane monooleate,[28, 29] and polymers including dextran, polyacrylamide, polyethyleneimine (PEI), poly(diallyldimethylammonium) chloride, poly(vinylalcohol), polyethylene glycol (PEG) and polyvinylpyrrolidone (PVP).[14, 30–32] The mechanism of stabilization includes electrostatic repulsion (e.g. citrate-coated and PEI-coated AgNPs), and steric repulsion (e.g. PEG and PVP-coated AgNPs).

Most capping agents, however are non-biodegradable polymers or potentially toxic chemicals, with the exception of polysaccharides. To disperse and stabilize AgNPs in aqueous solution with a nontoxic stabilizer, another promising strategy is to immobilize them with a biodegradable nanoparticle that is readily dispersible in water, such as cellulose nanocrystal (CNC), a rod-like nanoparticle that possesses high mechanical strength, biodegradability and biocompatibility.[33–35] CNC is produced from biomass via hydrolysis in strong acids, such as hydrochloric or sulfuric acids[36] and has dimensions of 5-10 nm in diameter and 200-400 nm in length.[37] This material has demonstrated numerous applications as hydrogels,[38–40] drug carriers,[41–44] reinforcing nanofillers[45, 46] and sorbents[47, 48]. As one of the most promising applications based on their large surface area, ~500 m^2/g, [49] CNC is an ideal subsrate for catalyst immobilisation in aqueous media.

To immobilize and stabilize nanoparticles on CNC, the adhesive characteristic of CNC surface must be improved. A facile and effective approach is to use dopamine, an emerging mussel-inspired coating material for organic and inorganic surfaces. The surface modification of materials with polydopamine (PD) can introduce a versatile chemical coating, yielding a surface with strong adsorption for most metallic

nanoparticles.[50] The resultant PD also possesses excellent reduction and chelation properties towards metal ions.[50] Thus, nanoparticles can be generated and subsequently anchored by in-situ reduction of corresponding metal salt on CNC surface.[51] By combining the remarkable adhesability of PD and excellent dispersibility of CNC, a nanoparticle dispersion with high stability could be achieved. Therefore, the catalytic and antibacterial properties of nanoparticle could be enhanced due to the greatly improved stability.

Here, the AgNPs were employed as a model material to demonstrate this new strategy. The stability and antimicrobial properties of AgNP immobilized polydopamine coated CNC (AgNP-PD-CNC) were evaluated. The stability was estimated by comparing the settling behavior of AgNP and AgNP-PD-CNC systems. The antimicrobial ability was estimated using *Escherichia coli* (Gram-negative) and *Bacillus subtilis* (Gram-positive) bacteria. The results revealed that the AgNP-PD-CNC remained stable in water for more than 3 months, while free AgNPs typically settled to the bottom within 24 hours. The antimicrobial activity of the resultant AgNP-PD-CNC was almost four times greater than AgNPs under the same experimental conditions.

Experimental

Materials and methods

CNC was supplied by CelluForce Inc. and used as received. The approximate dimensions are 5-10 nm diameter and length of 200-400 nm, with a specific surface area of approximately 500 m^2/g. Dopamine hydrochloride, silver nitrate, ammonia hydroxide solution, and tris((hydroxymethyl)aminomethane) were purchased from Sigma-Aldrich Co. Nutrient broth powder (OptiGrow™ Preweighed LB Broth, Lennox) was purchased from Thermo Fisher Scientific Inc. Plate Count Agar (DifcoTM Ref. 247940) was purchased from Becton Dickinson and Company. HeLa cell line was obtained from the American Type Culture Collection (ATCC, MD, USA). The cell was cultured in DMEM/F12 media containing 10% FBS, 100 U/mL penicillin, 100 µg/mL streptomycin at 37°C and, using humidified 5% CO_2 incubator. All the chemicals were used as received. *E. coli* and *B. subtilis* bacteria were purchased from Cedarlane Laboratories, in Burlington, Ontario. UV-Visible spectroscopy was performed using an Agilent 8453 UV-visible Spectroscopy system. Transmission electron microscopic (TEM) characterization was performed using a Philips CM10 electron microscope. The samples were prepared by spraying the aqueous solution (0.005 wt% solid) onto a carbon coated copper grid, and air-dried overnight at room temperature. Zeta-potential and particle size was measured with a Zetasizer (Malvern, Nano ZS90). Thermogravimetric analysis (TGA) was performed using the TGA Q600 of TA Instruments (New Castle, Delaware). The experiments were carried out under dry nitrogen purge at a flow rate of 10 mL/min from room temperature to 800 ºC at 15 ºC /min.

Preparation of polydopamine coated CNC (PD-CNC)

The coating process was adopted using a previously reported protocol.[51, 52] A typical procedure is described as follows: 1.0 g of CNC was dispersed in 500 mL deionized water using an IKA T25 homogenizer, followed by the addition of 0.6 g of tris((hydroxymethyl)aminomethane) to adjust the pH to 8.0. Then, 1.0 g of dopamine hydrochloride was added. The reaction was performed at room temperature for 2 days. At the end of the reaction, the products were purified in an ultrafiltration cell equipped with a 0.1µm pore size filtration membrane and washed several times with 200 mL deionized water until the filtrate became clear. The morphology of the resultant PD-CNC was determined by TEM and an example is shown in Fig. 1. The surface charge was determined by zeta-potential analyser and the results are summarized in Table 1.

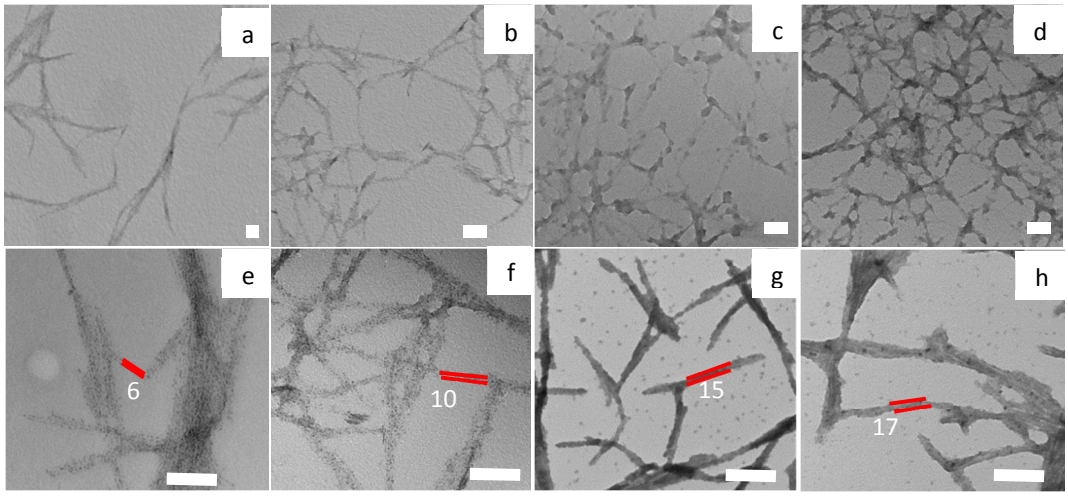

Fig. 1 TEM images of CNC (a, e) and PD-CNC with different feed ratios of PD:CNC = 0.5:1 (b, f), 1:1 (c, g) and 2:1(d, h). All the scale bars are 100 nm. Note: All the TEM images from bottom row were taken by staining PD-CNC with $FeCl_3$ to enhance the contrast.

Table 1. Zeta-potential of CNC, PD-CNC and AgNP-PD-CNC at different pHs

pH		3.50	4.52	5.55	6.86	9.81	10.81
zeta-potential (mV)	CNC	-36.8 ±4.09	-39.3 ±3.9	-42.9 ±5.05	-43.3 ±4.8	-39.1 ±4.85	-39.1 ±4.62
	PD-CNC	-8.3 ±1.66	-12.1 ±1.4	-18.6 ±1.91	-31.6 ±2.46	-32.6 ±2.25	-32.7 ±2.16
	AgNP-PD-CNC	-22.5 ±2.75	-31.4 ±3.9	-37.7 ±7.2	-37.4 ±5.3	-36.2 ±6.4	-35.5 ±5.4

Growing AgNPs on the surface of PD-CNC

The process was adopted from a modified version reported previously.[50] A typical protocol for preparing AgNPs on the surface of PD-CNC is described here: 50.0 mg of silver nitrate was introduced into 20 mL deionized water, and a 3.0 wt% ammonia solution was slowly added to the solution until the solution became clear indicating that diamine silver (I) was formed. Then 0.5 g of PD-CNC solution (3.0 wt%) was added to the resultant solution and stirred at room temperature for 1 h followed by the addition of 4.0 mg of dopamine hydrochloride (in 1.0 mL deionized water) that facilitated the reduction of silver ion. After 30 min, the product was purified by centrifugation at 8000 rpm for 10 min, and then washed with deionized water 3 times. The final product was characterized by TEM (Fig. 2), UV-Visible Spectroscopy (Fig. 3) and TGA (Fig. 4). As a control, free AgNP was prepared under similar conditions without PD-CNC, and they were characterized by DLS using the Zeta-sizer and TEM (Fig. 2). The dispersibility of AgNP-PD-CNC and AgNP was compared by dispersing them in water (32 μg/mL), and then photographs were taken after 24h and 3 months as shown in Fig. 5.

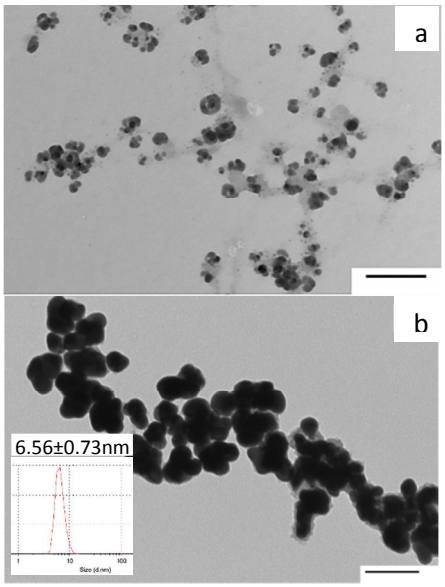

Fig. 2 TEM images of AgNP-PD-CNC (a) and pure AgNP (b). The insert picture shows the size distribution of AgNP by DLS data. All the scale bars are 100 nm.

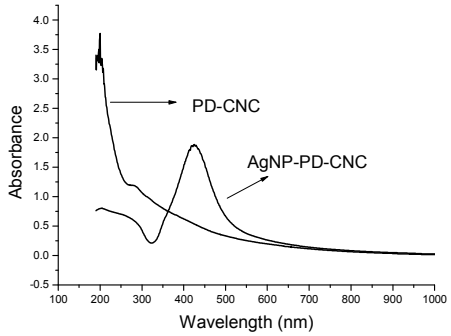

Fig. 3 UV spectra of PD-CNC and AgNP-PD-CNC.

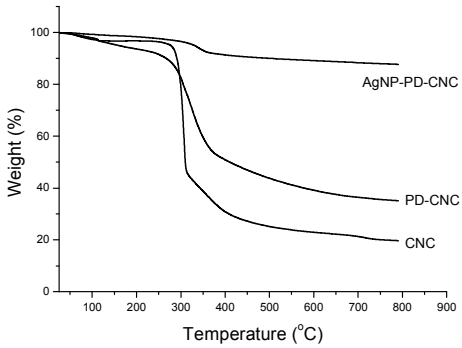

Fig. 4 TGA curves of CNC, PD-CNC and AgNP-PD-CNC

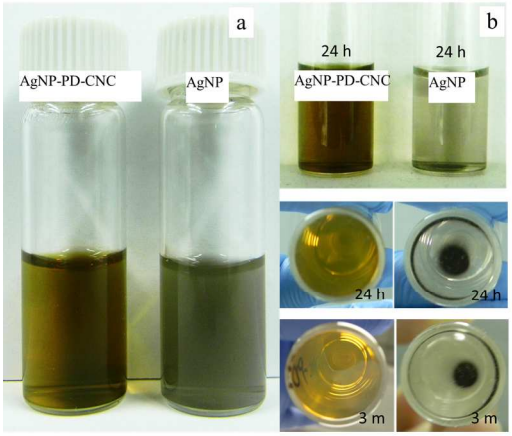

Fig. 5 Solutions of AgNPs and AgNP-PD-CNC immediately after preparation (a), and after one day and 3 months (b).

Antibacterial evaluation

The antibacterial activity of the resultant AgNPs and AgNP-PD-CNC was evaluated by determining the minimum inhibitory concentration (MIC) for Gram-negative (*E. coli*) and Gram-

positive (*B. subtilis*) bacteria, respectively. The detailed protocol is described below:

1) Agar plates and nutrient broth (2.0 g/L) preparation.

Agar powder (11.75 g) was dissolved in 500 mL deionized water, and 1.0 g nutrient broth was dissolved in 500 mL deionized water, and both were then sterilized in an autoclave for 30 min. The agar plates were prepared with the hot agar solution in a sterile environment using sterilized Petri dishes that were stored at 4°C prior to use.

2) Bacterial cultures.

First, the bacteria was cultured in LB nutrient broth at 35°C for 12 h and then the bacterial solution was diluted with LB broth until the optical density was between 0.07-0.08 at 600 nm.

3) Antibacterial solution preparation.

The AgNP-PD-CNC and free AgNPs solutions were prepared in concentrations ranging from 0.5 to 32 μg/mL, where all the concentrations were calculated based on the mass of AgNPs. The mass of PD-CNC was deducted from AgNP-PD-CNC, so that the AgNPs solution and AgNP-PD-CNC solution possessed the same weight concentration based on the mass of silver.

4) Incubation.

LB nutrient broth (1.0 mL) was mixed with 1.0 mL AgNP-PD-CNC solution and 10 μL of bacteria solution in a sterilized 15 mL plastic centrifuge tube. The control sample was prepared using the same protocol, but the AgNP-PD-CNC solution was replaced by deionized water. The solution was then placed onto a rotary shaker at 90 rpm and maintained at 37 °C for 4 hrs.

5) Antibacterial property evaluation.

After incubation, 0.1 mL of the bacterial solution was transferred to the surface of an agar plate in a sterile environment, and the solution was spread with a sterile glass rod to homogeneously cover the surface. Then all the agar plates were placed in an incubator for colony growth at 35 °C overnight.

The minimum inhibitory concentration (MIC) was determined according to the lowest AgNPs and AgNP-PD-CNC concentrations that inhibited the visible growth of microbes after incubation overnight. Photographs of bacterial colony growth in different concentrations of antimicrobial agents are shown in Fig. 6 and 7.

A preliminary study on the mechanism was performed by conducting TEM analysis of the bateria broth with the silver nanoparticles Only *E. coli* was studied as they could be easily imaged with the need for staining. The *E. coli* solution was first diluted with sterilized water until the optical density was between 0.07-0.08 at 600 nm. Then 0.1 mL solution of synthesized nanoparticle (250 μg/mL) was introduced into 0.9 mL *E. coli* solution, and the concentration of nanoparticle in the final solution was 25 μg/mL. The mixture was mixed for a predetermined duration in a shaking bed at 25°C, and one drop of the solution was placed on a carbon coated copper-grid and air-dried over night prior to the TEM analysis. The resultant TEM images are shown in Fig. 8.

Cytotoxicity evaluation

The procedure for evaluating the cytotoxicity of the resultant nanoparticles was performed according to the literature.[53] Typically, HeLa cells were seeded in 96-well plates filled with 5,000 cells per well in 100μL of cell medium, and incubated at 37 °C under 5% CO_2 humidified atmosphere for 24 h. Then, the culture medium was replaced with 100μL of freshly prepared culture medium containing AgNP or AgNP-PD-CNC with different nanoparticle concentrations. Here, ten concentrations were investigated. They are 50, 25, 12.5, 6.25, 3.12, 1.56, 0.78, 0.39, 0.19 and 0 μg/mL. The cells were further incubated for 72h, and then 25μL of MTT (3-(4,5-dimethylthiazol-2-yl)-2,5-diphenyltetrazolium bromide) stock solution (5 mg/mL in PBS) was added to each well to achieve a final concentration of 1 mg/mL, with the exception of the controlled "blank" wells, where 25μL of PBS was added. After incubation for another 2 h, 100 μL of extraction buffer (20% SDS in 50% DMF, pH=4.7, prepared at 37°C) was added to the wells and incubated for another 4 h at 37° C. The absorbance was measured at 570 nm using a SpectraMax M3 microplate reader. Cell viability was normalized to that of HeLa cells cultured in the cell media. Three repetitions were conducted for each concentration, and the results of the cell viability are summarised in Fig. 9.

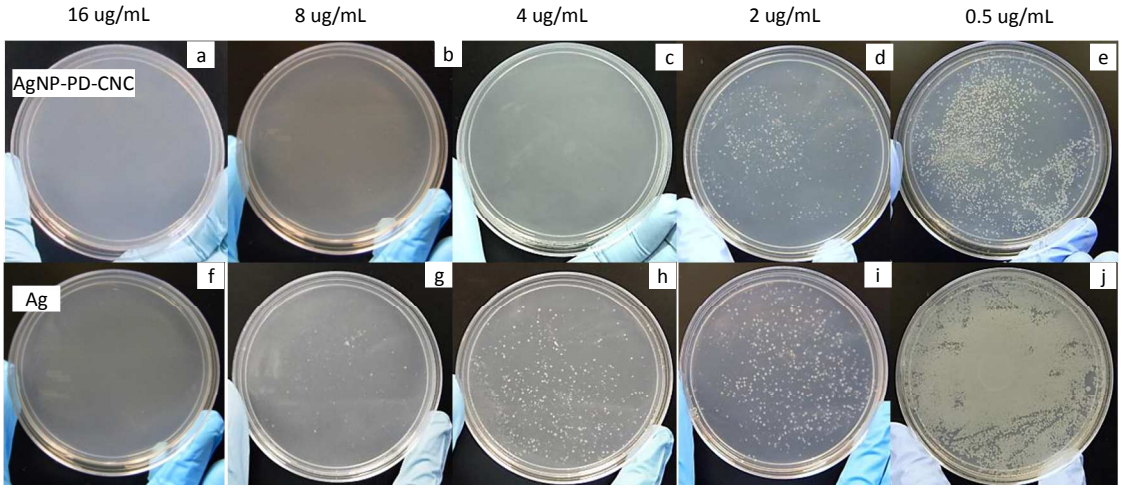

Fig. 6 Antimicrobial activity of AgNP-PD-CNC and AgNPs evaluated with *E. coli*. The antimicrobial agent concentrations are shown on the top of each plate. The plates in the top row show the colony growth with AgNP-PD-CNC, while the plates in the bottom row show the colony growth under free AgNP.

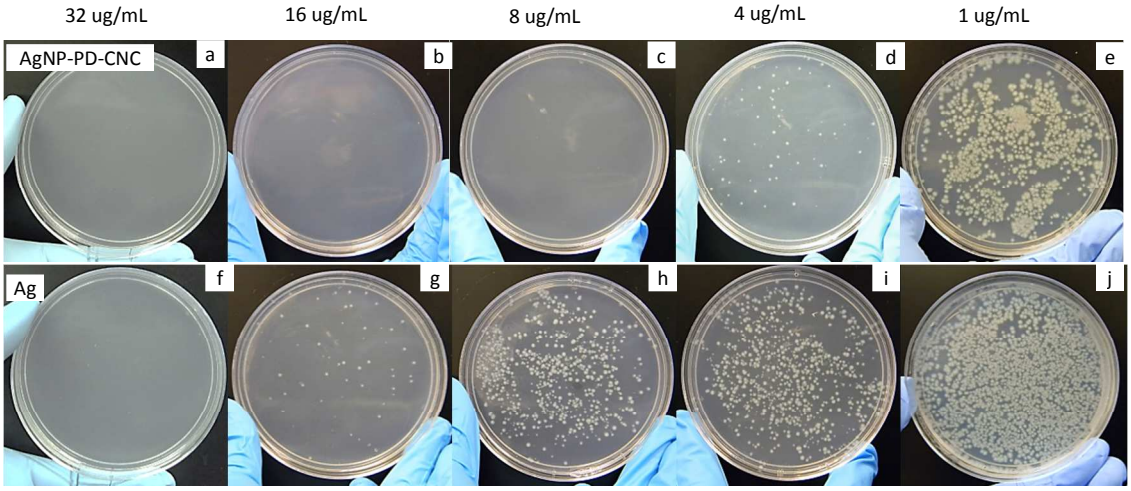

Fig. 7 Antimicrobial activity of AgNP-PD-CNC and AgNPs evaluated with *B. subtilis*. The antimicrobial agent concentrations are shown on the top of each plate. The plates in the top row show the colony growth with AgNP-PD-CNC, while the plates in the bottom row show the colony growth with free AgNP.

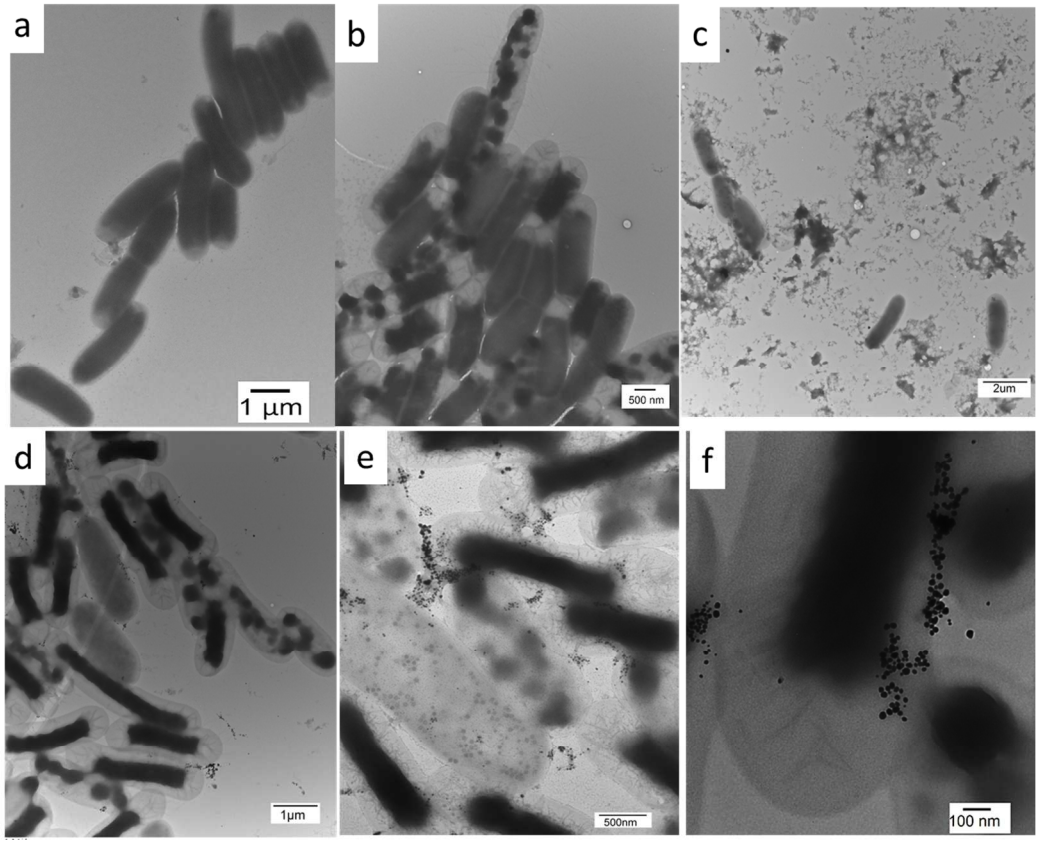

Fig. 8 TEM images of (a) *E. coli*.; (b) *E. coli*. mixed with AgNPs after 12h; (c) *E. coli*. mixed with AgNPs after 24h; (d) *E. coli*. mixed with AgNP-PD-CNC after 12h; (e) *E. coli*. mixed with AgNP-PD-CNC after 24h; (f) AgNPs attached on the surface of *E. coli*. at high magnification.

Cite this: DOI: 10.1039/coxx00000x

www.rsc.org/xxxxxx

PAPER

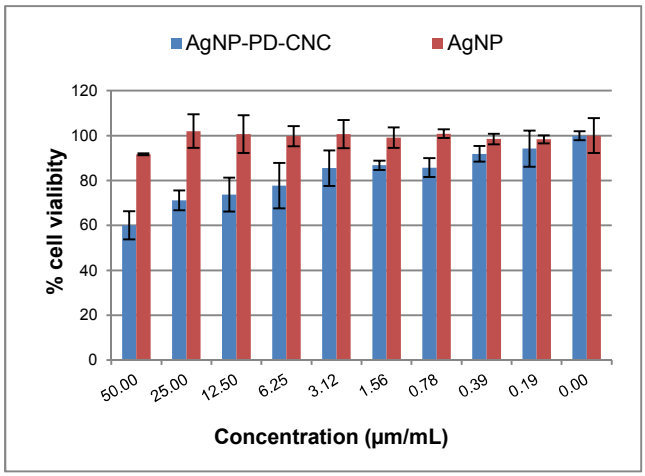

Fig. 9 Viability measured using MTT assay in the presence of free AgNP and AgNP-PD-CNC hybrid.

Results and discussion

Preparation of polydopamine coated CNC (PD-CNC)

Recently, the polymerization mechanism and structure of polydopamine was investigated in detail by Bielawski and co-workers using solid state spectroscopic and crystallographic techniques. The data analysis showed that polydopamine comprises of a supramolecular aggregate of monomers held together via charge transfer, π-stacking, and hydrogen bonding interactions.[54] The present study aims to use the polydopamine synthetic protocol to prepare a robust coating on the surface of cellulose nanocrystals (CNCs). The feed ratios of CNC to dopamine (DP) were first evaluated. Various feed ratios of DP:CNC = 0.5:1, 1:1 and 2:1 by weight were examined. The morphologies of the prepared PD-CNC were characterized by TEM and are shown in Fig. 1. From Figs. 1a-d, the PD-CNC displayed a better dispersibility in dried state on the copper grids. The magnified image in Fig. 1e showed a bundle-like structure consisting of several pristine CNC nanorods. In contrast, the PD modified CNC consisted of predominantly individual nanorods at all feed ratios, as shown in Figs. 1f-h.

The TEM images revealed that the diameter of individual PD-CNC was approximately 6 nm for pristine CNC, and 10, 15 and 17 nm for PD-CNC at feed ratios of DP:CNC = 0.5:1, 1:1, 2:1, respectively. Based on the TEM image, the diameter increased by 4 nm under the feed ratio of DP:CNC = 0.5:1, while it increased by 9 and 11 nm with the feed ratios of DP:CNC = 1:1 and 2:1, respectively. The diameter of PD-CNC did not increase any further even though the amount of DP was doubled. Hence, the feed ratio for preparation of PD-CNC was fixed at DP:CNC = 1:1.

The zeta-potential analysis is summarized in Table 1, and we observed that the surface of CNC, PD-CNC and AgNP-PD-CNC was all negatively charged at all pH values. The zeta-potential (ZP) for CNC remained constant at around – 40 mV. The ZP of PD-CNC decreased gradually with increasing pH and approached a stable value at approximate -32mV at pH greater than 7. The negative charges are attributed to the phenol groups on the dopamine molecules since phenol is a weak acid.

Preparation of AgNPs on the surface of PD-CNC

The growth of AgNP could be achieved by in-situ reduction of silver nitrate with PD-CNC.[55] The proposed mechanism for reduction of silver ion by dopamine is illustrated in Scheme 1 according to a previous report.[56] The morphology of the resultant AgNP-PD-CNC and pure AgNPs are shown in Fig. 2. It is clearly evident that all the AgNPs were deposited on the surface of PD-CNC as shown in Fig. 2a, while in Fig. 2b, pure AgNPs generated by dopamine tended to form large clusters when dried on the copper grid, which is consistent with the inherent aggregation characteristics of AgNPs.[57] The DLS data for AgNP shown in the inset in Fig. 2b indicated that the size of AgNPs in solution was around 6 nm, but they aggregated to form clusters of approximately 20-50 nm when dried.

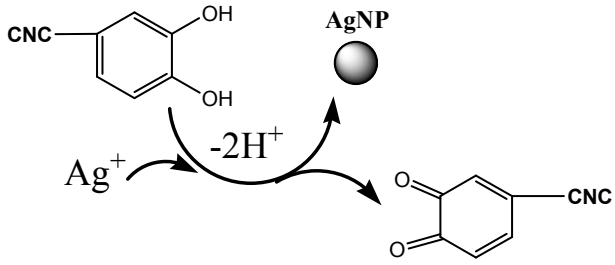

Scheme 1 A proposed reaction mechanism for reduction of silver nitrate by dopamine[56]

The successful production of AgNP was further confirmed by UV-Vis spectroscopy as shown in Fig. 3. The peak located near 420 nm in the spectrum is a typical peak for AgNPs.[58] Furthermore, the amounts of silver in AgNP-PD-CNC was determined by TGA and showed in Fig. 4. At 800°C, the residue was 20.0, 35.1 and 87.6% for pristine CNC, PD-CNC and AgNP-PD-CNC. Thus, the content of AgNP in AgNP-PD-CNC was calculated to be 81% based on the following equations:

$$C_{Ag} + C_{PD\text{-}CNC} = 1$$

$$C_{Ag} + 0.351C_{PD\text{-}CNC} = 0.876$$

where C_{Ag} is the content of silver in AgNP-PD-CNC and $C_{PD\text{-}CNC}$ is the amounts of PD-CNC in AgNP-PD-CNC system.

The dispersion stability of AgNP-PD-CNC and pure AgNPs is shown in Fig. 5. It is evident that for the solution of AgNP-PD-CNC, no sediment was observed (Fig. 5b), while for pure AgNP, significant agglomeration and precipitation occurred after 1 week (Fig. 5b). The results from visual pictures were consistent with

that observed from TEM images. Thus, the present study demonstrated that the preparation of AgNP on stable CNC significantly improved the dispersibility of AgNP and minimized agglomeration. An important consequence of this is that the large surface area of AgNPs is preserved, and this will have a positive impact on the performance of the nanoparticles in various applications, such as their antimicrobial property.

The zeta-potential results of AgNP-PD-CNC system (Table 1) showed that it decreased gradually with increasing pH, approaching a stable value of approximately -35mV at pH greater than 5.5. This is more negative than the PD-CNC system, which could be due to the reducing reaction of silver ions, as shown in Scheme 1, where some of the phenol groups on dopamine became oxidized and surface charge become more negative than PD-CNC.

Antibacterial Test

AgNPs, being very effective antimicrobial agents, are widely used in many products, although the mechanism of antimicrobial activity is not well understood.[19–21] Despite a comprehensive understanding on its activity, one of the key characteristics that contributes to its excellent performance in solution is the dispersion stability. Here, we compared the impact of pure AgNPs and the AgNP-PD-CNC hybrid on the antibacterial activity against two bacteria, one Gram-negative (*E. coli*) and one Gram-positive (*B. subtilis*).

For the *E. coli* system, the impact of the two AgNP preparations on the growth of bacterial colonies is shown in Fig. 6, where the density of colonies decreased with increasing AgNP concentration. The *E. coli* colonies were completely eliminated when the concentration of AgNP-PD-CNC was 4 μg/mL (Fig. 6c), while for the pure AgNP solution the same effect required four times the concentration, i.e. 16 μg/mL (Fig. 6f). The MIC for pure AgNP was between 8-16 μg/mL compared to 2-4 μg/mL for AgNP-PD-CNC. Therefore the antibacterial activity of AgNP-PD-CNC was approximately four times better than AgNP when the same mass of silver was used with *E. coli*.

The antibacterial MIC test results for *B. subtilis* are shown in Fig. 7. From the pictures, the density of bacterial colonies decreased gradually along with the increase of AgNP concentration. The colonies were completely eliminated when the concentration of AgNP-PD-CNC was 8 μg/mL (Fig. 7c). For pure AgNP samples, the colonies disappeared only when the concentration was 32 μg/mL (Fig. 7f). The MIC for pure AgNP was between 16-32 μg/mL, and it was 4-8 μg/mL for AgNP-PD-CNC. Thus, the antibacterial activity of AgNP-PD-CNC was about four times better than that of AgNP for *B. subtilis*, similar to the results found for *E. coli.*

Comparison of the antibacterial property (i.e. MIC) with other systems performed under the same conditions is documented in Table 2.[58] All AgNPs possessed a comparable primary particle size of approximately 7 nm. In the absence of surfactants, the AgNPs were agglomerated, while the AgNP-PD-CNC was stable due to the highly charged CNC. The results indicated that for *E. coli*, the AgNP-PD-CNC possessed a MIC value of 4 μg (Ag)/mL, which is approximately four times lower than that of the reference reported. As for the *B. subtilis*, the MIC of AgNP-PD-CNC was 8 μg (Ag)/mL, again almost four times lower than previously reported. All the MIC values in the reference are similar to the results from pure AgNP prepared in our system.

Table 2. Comparison of MIC for AgNP-PD-CNC and pure AgNP

Bacterium	MIC (μg(Ag)/mL) (reference 59)	MIC (μg(Ag)/mL) (AgNP-PD-CNC)	MIC (μg(Ag)/mL) (Free AgNP)
E. coli	20	4	16
B. subtilis	40	8	32

Note: all AgNPs has an average particle size around 7 nm based on the reference description,[59] TEM (Fig. 2a) and DLS (Fig.2b insert).

As shown in Table 2, the AgNP-PD-CNC system displayed antibacterial activity that was four times better than pure AgNPs on both the Gram-positive and Gram-negative bacteria. The improved antibacterial activity was attributed to the improved dispersion of AgNP when they were incorporated onto PD-CNC.

To understand the improved antimicrobial properties of AgNP-PD-CNC system, a TEM study was conducted. Comparing the results from AgNP and AgNP-PD-CNC systems, shown in Fig. 8, we found that after 12h treatment, the morphology of AgNPs treated bacteria did not change significantly compared to the pristine bacteria (Fig. 8a vs. Fig. 8b) and AgNPs were not observable from the TEM images (Fig.8b). The morphology of AgNP-PD-CNC hybrid nanoparticles treated bacteria was quite different. It was clearly visible that the dark region inside the cell became smaller, and a translucent shell was observed, suggesting cell death and the degradation of the biological matter that migrated to the inner core of the cell. For example, the original cell possessed a uniform dark core, while the AgNP-PD-CNC hybrid treated cell (Fig. 8d) showed a shrunken rectangle-like dark core (Fig. 8a). It is also evident that the AgNP-PD-CNC nanoparticles were adhering to the bacteria cell wall and released silver ions that readily diffused into the bacteria cell compartment. For the normal AgNP nanoparticles, we hypothesized that the nanoparticles might have entered the cell as they were not present outside the bacteria cell. By comparing the images after 24h treatment (Fig. 8c and Fig. 8e), small fragments probably due to disrupted bacteria cell walls were observed compared to the more defined bacteria cell structure in Fig.8e. Based on the TEM analyses and previous reported results,[60-62] we propose the most probable mechanisms for the antimicorbial activity of the two different AgNP systems. For pure AgNP nanoparticles, the nanoparticles are internalized into the bacteria cell, and the combined effect of cell wall breakage and silver ions chelating with peptides that hinder the replication activity of the bacteria.[60-62] In the case of AgNP-PD-CNC hybrid system, the large particle size and the adhesive property of PD caused the nanoparticle to adhere on the surface of bacteria, and high concentration of silver ions are then released from the localised AgNP-PD-CNC nanoparticles.

Cytotoxicity evaluation

The cytotoxicity tests of the resultant nanoparticles were performed using HeLa cell. In Fig. 9, both AgNP and AgNP-PD-CNC hybrid showed some toxicity to HeLa cells. For AgNP, beyond a concentration of 50μg/mL around 10% of cell death was observed, and no toxicity was observed at lower AgNP concentration. For the AgNP-PD-CNC hybrid, around 10% of cell death was observed when the concentration exceeded 3μg/mL, while at 50 μg/mL, around 40% of the cells were not viable. Since the cell line used is that of cancer cell, AgNP-PD-

CNC hybrid was shown to possess anti-cancer characteristics, which could be beneficial in some situation. The reasons why the AgNP-PD-CNC hybrid system displayed higher toxicity to HeLa cell since the AgNP-PD-CNC hybrid system is more stable and can adhere to the surface of the cell and release silver ions near the cell membrane.

Conclusions

The present study focuses on producing well-dispersed silver nanoparticles on the surface of CNC. A versatile mussel-inspired dopamine system was employed to functionalize water-dispersible and biocompatible CNC in a facile and effective way to yield polydopamine coated CNC. Then, the polydopamine coated CNC could reduce silver ions to form AgNP on the surface of PD-CNC. The improved stability was demonstrated by comparing the AgNP-PD-CNC system and free AgNP. The high stability of AgNP-PD-CNC system displayed antimicrobial activity that is four times better than free AgNP system against both Gram-positive and Gram-negative bacteria. TEM analyses indicated that AgNP may enter the cell and disrupt the cell membrane, while the AgNP-PD-CNC hybrid only adheres on surface of cell due to the adhesive property of polydopamine. Further studies are on going to elucidate and clarify the antibacterial mechanism of these nanomaterials.

Acknowledgements

We wish to acknowledge Celluforce Inc. for providing the cellulose nanocrystals. The research funding from CelluForce and AboraNano facilitated the research on CNC. K. C. Tam wishes to acknowledge funding from CFI and NSERC.

Notes and references

[a] *Department of Chemical Engineering, Waterloo Institute for Nanotechnology, University of Waterloo, 200 University Ave. W, Waterloo, Ontario, Canada N2L 3G1. Fax: 1-519-888-4347; Tel: 1-519-888-4567 x38339; E-mail: mkctam@uwaterloo.ca*
[b] *CelluForce, Inc., 625 President-Kennedy Ave., Montreal, Quebec, Canada H3A 1K2.*

References:

1. A. Kumar, P. K. Vemula, P. M. Ajayan and G. John, *Nat. Mater.*, 2008, **7**, 236.
2. D. M. Eby, H. R. Luckarift and G. R. Johnson, *ACS Appl. Mater. Interfaces*, 2009, **1**, 1553.
3. M. Ahamed, M. S. Alsalhi and M. K. J. Siddiqui, *Clin. Chim. Acta.*, 2010, **411**, 1841.
4. S. Chernousova, M. Epple, *Angew. Chem. Int. Ed. Engl.*, 2013, **52**, 1636.
5. D. I. Tee, M. Mariatti, A. Azizan, C. H. See and K. F. Chong, *Compos. Sci. Technol.*, 2007, **67**, 2584.
6. B. K. Kuila, A. Garai and A. K. Nandi, *Chem. Mater.,* 2007, **19**, 5443.
7. K. Y. Chun, Y. Oh, J. Rho, J. H. Ahn, Y. J. Kim, H. R. Choi and S. Baik, *Nat. Nanotechnol.*, 2010, **5**, 853.
8. K. Aslan, M. Wu, J. R. Lakowicz and C. D. Geddes, *J. Am. Chem. Soc.*, 2007, **129**, 1524.
9. Y. Lu, G. L. Liu and L. P. Lee, *Nano Lett.*, 2005, **5**, 5.
10. M. Zhu, C. Wang, D. Meng and G. J. Diao, *Mater. Chem. A*, 2013, **1**, 2118.
11. E. K. Jeon, E. Seo, E. Lee, W. Lee, M. K. Um and B. S. Kim, *Chem. Commun.*, 2013, **49**, 3392.
12. L. Ai, H. Yue and J. Jiang, *J. Mater. Chem.*, 2012, **22**, 23447.
13. M. Rai and A. Yadav, A. Gade, *Biotechnol. Adv.*, 2009, **27**, 76.
14. V. K. Sharma, R. Yngard and Y. Lin, *Adv. Colloid Interface Sci.*, 2009, **145**, 83.
15. W. K. Jung, H. C. Koo, K. W. Kim, S. Shin, S. H. Kim and Y. H. Park, *Appl. Environ. Microbiol.*, 2008, **74,** 2171.
16. S. Prabhu and E. K. Poulose, *Int. Nano Lett.*, 2012, **2**, 32.
17. R. Zhang, K. Eggleston, V. Rotimi and R. J. Zeckhauser, *Global. Health*, 2006, **2**, 6.
18. T. Dankovich and D. G. Gray, *Environ. Sci. Technol.*, 2011, **45**, 1992.
19. F. Mohammed, K. Balaji, M. Girilal, P. T. Kalaichelvan and R. J. Venkatesan, *Agric. Food Chem.*, 2009, **57**, 6246.
20. P. Rujitanaroj, N. Pimpha and P. Supaphol, *Polymer*, 2008, **49**, 4723.
21. S. Kokura, O. Handa, T. Takagi, T. Ishikawa, Y. Naito and *T.* Yoshikawa, *Nanomedicine*, 2010, **6**, 570.
22. N. Durán, P. D. Marcato, G. I. H. De Souza, O. L. Alves and E. J. Esposito, *Biomed. Nanotechnol.*, 2007, **3**, 203.
23. A. Henglein and M. J. Giersig, *Phys. Chem. B*, 1999, **103**, 9533.
24. Y. Wang and H. Yang, *Chem. Commun*., 2006, 2545.
25. Y. Park, Y. N. Hong, A. Weyers, Y. S. Kim and R. J. Linhardt, *IET Nanobiotechnol.*, 2011, **5**, 69.
26. S. Singh, P. Patel, S. Jaiswal, A. A. Prabhune, C. V. Ramana and B. L. V. Prasad, *New J. Chem.*, 2009, **33**, 646.
27. J. E. Song, T. Phenrat, S. Marinakos, Y. Xiao, J. Liu, M. R. Wiesner and R. D. Tilton, G. V. Lowry, *Environ. Sci. Technol*., 2011, **45**, 5988.
28. L. Kvitek, A. Panacek, J. Soukupova, M. Kolar, R. Vecerova, R. Prucek, M. Holecova and R. J. Zboril, *Phys. Chem. C*, 2008, **112**, 5825.
29. J. Soukupová, L. Kvítek, A. Panáček, T. Nevěčná and R. Zbořil, *Mater. Chem. Phys*., 2008, **111**, 77.
30. P. Dallas, V. K. Sharma, R. Zboril, *Adv. Colloid Interface Sci.*, 2011, **166**, 119.
31. R. Eising, A. M. Signori, S. Fort and J. B. Domingos, *Langmuir*, 2011, **27**, 11860.
32. A. M. El Badawy, T. P. Luxton, R. G. Silva, K. G. Scheckel, M. T. Suidan and T. M. Tolaymat, *Environ. Sci. Technol*., 2010, **44**, 1260.
33. Y. Habibi, L. A Lucia and O. J. Rojas, *Chem. Rev.*, 2010, **110**, 3479.
34. B. L. Peng, N. Dhar, H. L. Liu and K. C. Tam, *Can. J. Chem. Eng*., 2011, **89**, 1191.
35. S. J. Eichhorn, *Soft Matter*, 2011, **7**, 303.
36. E. Lam, K. B. Male, J. H. Chong, A. C. W. Leung and J. H. T. Luong, *Trends Biotechnol*., 2012, **30**, 283.
37. S. Beck, J. Bouchard and R. Berry, *Biomacromolecules*, 2011, **12**, 167.
38. R. Sanna, E. Fortunati, V. Alzari, D. Nuvoli, A. Terenzi, M. F. Casula, J. M. Kenny and A. Mariani, *Cellulose*, 2013, **20**, 2393.
39. C. Zhou, Q. Wu, Y. Yue and Q. J. Zhang, *Colloid Interface Sci.*, 2011, **353**, 116.
40. J. Yang, C. R. Han, J. F. Duan, M. G. Ma, X. M. Zhang, F. Xu, R. C. Sun and X. M. Xie, *J. Mater. Chem.*, 2012, **22**, 22467.
41. H. Wang, C. Qian and M. Roman, *Biomacromolecules*, 2011, **12**, 3708.
42. N. Drogat, R. Granet, C. Le Morvan, G. Bégaud-Grimaud, P. Krausz and V. Sol, *Bioorg. Med. Chem. Lett.*, 2012, **22**, 3648.
43. N. Lin, A. Dufresne, *Biomacromolecules*, 2013, **14**, 871.
44. S. P. Akhlaghi, R. C. Berry and K. C. Tam, *Cellulose*, 2013, **20**, 1747.
45. J. D. Fox, J. R. Capadona, P. D. Marasco and S. J. Rowan, *J. Am. Chem. Soc.*, 2013, **135**, 5167.
46. J. Fox, J. J. Wie, B. W. Greenland, S. Burattini, W. Hayes, H. M. Colquhoun, M. E. Mackay and S. J. Rowan, *J. Am. Chem. Soc.*, 2012, **134**, 5362.
47. R. Batmaz, N. Mohammed, M. Zaman, G. Minhas, R. M. Berry and K. C. Tam, *Cellulose*, 2014, **21,** 1655.
48. L. Chen, R. M. Berry and K. C. Tam, *ACS Sustain. Chem. Eng*., 2014, **2**, 951.
49. L. Heath and W. Thielemans, *Green Chem.*, 2010, **12**, 1448.

50. Y. Liu, K. Ai and L. Lu, *Chem. Rev*., 2014, *114*, 5057.
51. Z. Zhang, J. Zhang, B. Zhang and J. Tang, *Nanoscale*, 2013, **5**, 118.
52. H. Lee, S. M. Dellatore, W. M. Miller and P. B. Messersmith, *Science*, 2007, **318**, 426.
53. F. Wang and J. Liu, *Small*, 2014, **10**, 3927.
54. D. R. Dreyer, D. J. Miller, B. D. Freeman, D. R. Paul and C. W. Bielawski, *Langmuir*, 2012, **28**, 6428.
55. Y. Jiang, Y. Lu, L. Zhang, L. Liu, Y. Dai and W. J. Wang, *Nanoparticle Res*., 2012, **14**, 938.
56. H. Niu, S. Wang, T. Zeng, Y. Wang, X. Zhang, Z. Meng and Y. Cai, *J. Mater. Chem*., 2012, **22**, 15644.
57. V. K. Sharma, K. M. Siskova, R. Zboril and J. L. Gardea-Torresdey, *Adv. Colloid Interface Sci*., 2014, **204**, 15.
58. Y. Sun and Y. Xia, *Science*, 2002, **298**, 2176.
59. S. Agnihotri, S. Mukherji and S. Mukherji, *RSC Adv.*, 2014, **4**, 3974.
60. S.Mukherjee, D. Chowdhury, R. Kotcherlakota, S. Patra, Vinothkumar B, M. P. Bhadra, B. Sreedhar and C. R. Patra, *Theranostics*, 2014, **4**, 316.
61. S. Shrivastava, T. Bera, A. Roy, G. Singh, P. Ramachandrarao and D. Dash, *Nanotechnology*, 2007, **18**, 225103.
62. J. R. Morones, J. L. Elechiguerra, A. Camacho, K. Holt, J. B Kouri, J. T. Ramırez and M. J. Yacaman, *Nanotechnology*, 2005, **16**, 2346.

TOC

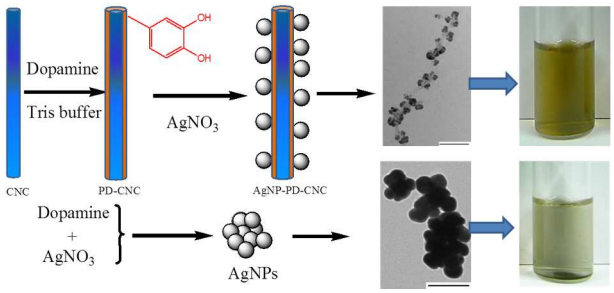

Preparation of polydopamine functionalized CNC and silver nanoparticle immobilized CNC